Int. J. Nav. Archit. Ocean Eng. (2015) 7:995~1006
http://dx.doi.org/10.1515/ijnaoe-2015-0069
pISSN: 2092-6782, eISSN: 2092-6790

Parametric geometric model and shape optimization of an underwater glider with blended-wing-body

Chunya Sun, Baowei Song and Peng Wang

School of Marine Science and Technology, Northwestern Polytechnical University, Xi'an, China

Received 18 March 2015; Revised 8 July 2015; Accepted 12 August 2015

ABSTRACT: *Underwater glider, as a new kind of autonomous underwater vehicles, has many merits such as long-range, extended-duration and low costs. The shape of underwater glider is an important factor in determining the hydrodynamic efficiency. In this paper, a high lift to drag ratio configuration, the Blended-Wing-Body (BWB), is used to design a small civilian under water glider. In the parametric geometric model of the BWB underwater glider, the planform is defined with Bezier curve and linear line, and the section is defined with symmetrical airfoil NACA 0012. Computational investigations are carried out to study the hydrodynamic performance of the glider using the commercial Computational Fluid Dynamics (CFD) code Fluent. The Kriging-based genetic algorithm, called Efficient Global Optimization (EGO), is applied to hydrodynamic design optimization. The result demonstrates that the BWB underwater glider has excellent hydrodynamic performance, and the lift to drag ratio of initial design is increased by 7% in the EGO process.*

KEY WORDS: Underwater glider; Blended-wing-body; Shape optimization; Computational fluid dynamics (CFD), Sensitivity.

INTRODUCTION

Underwater glider is a type of Autonomous Underwater Vehicles (AUVs) that glides through the ocean by controlling their buoyancy and converting the lift on wings into propulsive force to propel themselves forward (Bachmayer et al., 2004). Since the concept of underwater glider was envisioned in 1989 (Stommel, 1989), many underwater gliders, such as the Slocum glider (Webb et al., 2001), the Spray glider (Sherman et al., 2001), and the Seaglider (Eriksen et al., 2001) et al., have many useful applications in oceanographic sensing and data collection (Graver, 2005).

The advantages of gliders, such as low cost, capability for long-range and extended-duration deployments, rely on the shape which has excellent hydrodynamic performance. The configurations of conventional underwater gliders have revolving body, wings and control surfaces. The most common revolving body is a cylinder with Semi-elliptical head and tail, such as the Slocum glider and the Spray glider. Another revolving body used by the Seaglider is the fully appended laminar flow body (Huggins and Packwood, 1995), and the dragof this body is lower than the common revolving body. Although the drag of revolving bodies is continuously reduced by some research works (Stevenson et al., 2009; Ma et al., 2006), these bodies cannot provide high lift like wings.

Corresponding author: *Peng Wang*, e-mail: *791485913@qq.com*

For achieving higher hydrodynamic efficiency, a flying wing design, Liberdade XRAY, was developed by U.S. Office of Naval Research (ONR, 2006). The flying wing design significantly improves its maximum lift to drag ratio by eliminating the body of the glider, but its interior space contained within the wing section becomes so narrow that it is difficult to incorporate more components, like batteries, within a flying wing (Graver, 2005).

In aviation, the BWB configurations, that have been studied by many institutes (Liebeck, 2004; Peigin and Epstein, 2006; Mohr et al., 2012; Li et al., 2012), were proposed based on flying wing designs (Potsdam et al., 1997). These configurations have no clear dividing line between the wings and the main body of the craft. The body form is composed of distinct and separate wing structures, though the wings are smoothly blended into the body, unlike a flying wing which has no distinct fuselage (Crane, 2012). The advantage of this configuration lies in higher maximum lift to drag ratio and lower wetted area to volume ratio, and this advantage is also applicable to underwater gliders. Jenkins et al. (2003) have fully studied the feasibility of BWB underwater gliders, and they provided a guidance to ONR. In 2010, the latest generation "Liberdade ZRay" model, which is a blended wing body design and the world's largest known underwater glider, was completed by ONR (Hildebrand et al., 2011).

In this paper, the conceptual design of a small civilian BWB under water glider, which weighs about 50-70 *kg*, is discussed. In three dimensional modeling process the wings are smoothly blended into a disk body, which has higher hydrodynamic performance (Liebeck, 2004), by Bezier curve (Prautzsch et al., 2002). This research focuses on studying the effect of geometric parameters on the hydrodynamic performance and achieving higher maximum lift to drag ratio by a CFD-driven optimization. The hydrodynamic numerical simulation has been performed by the commercial code Fluent with the incompressible Navier-Stokes equations. The kriging-based genetic algorithm, called Efficient Global Optimization (EGO) (Jeong et al., 2005), is applied to this expensive black-box function optimization.

GEOMETRY CONFIGURATION

In the BWB configuration of this under water glider, the disk body is blended and smoothed into the wings, and it is also a wing and a pitch control surface as shown in Fig. 1(a). This reduces interference drag and provides additional effective wing chord at the wing-body junction. Because our BWB underwater glider is designed to glide up and down at the same glide path angle and speed, its body and wings are top-to-bottom symmetrical. This is advantageous that gliding performance is the same gliding up or down as shown Fig. 1(b). The BWB Underwater Glider geometry proposed in this study includes planform and relative thickness distribution.

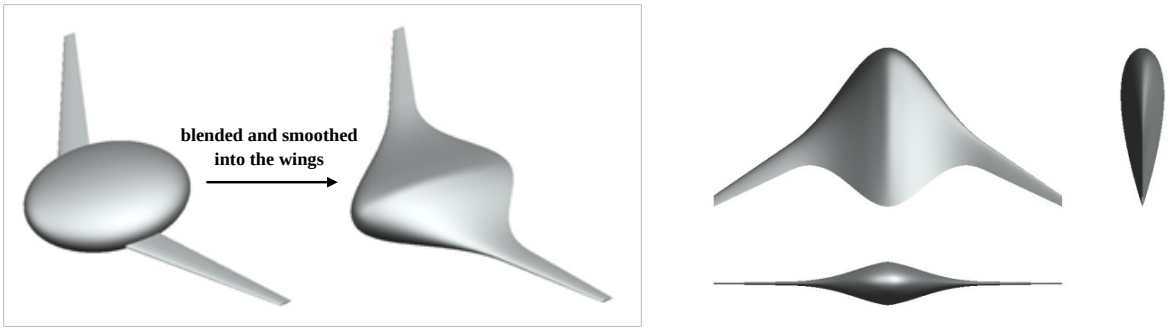

(a) (b)

Fig. 1 the BWB underwater glider: (a) (b).

Parameters of planform

Fig. 2 shows the definition of the BWB's planform. The oval body is blended and smoothed into the wing by two cubic Bezier curves (Farin and Kim, 2002). Each cubic Bezier curve is drawn by four control points, and z_1– z_3 represent the spanwise coordinate of the control points.

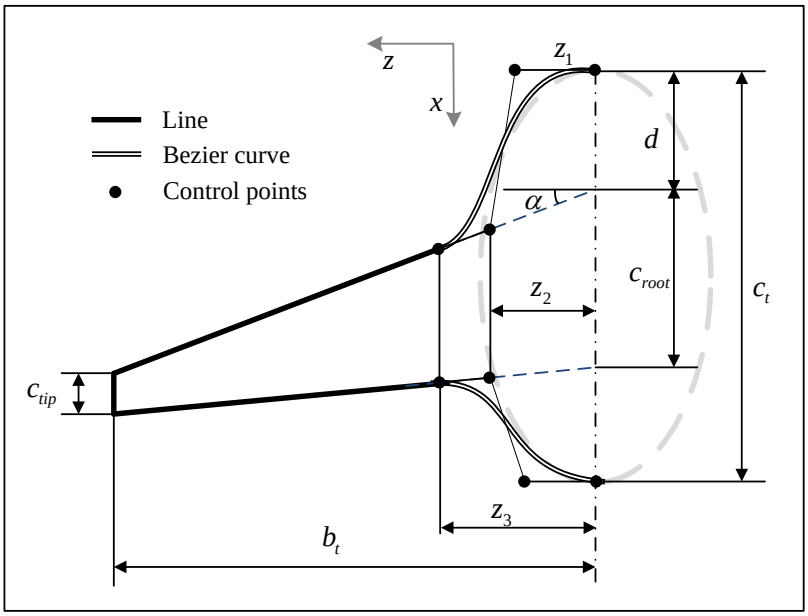

Fig. 2 Definition of planform.

In order to determine the BWB's planform, we define 8 non-dimensional parameters that include 4 wing parameters and 4 body parameters as shown in Table 1.

Table 1 Parameters of planform.

Parameter	Explanation	Equation
Wing parameters		
AR	Aspect ratio	$AR = b_t / c_t$
TR	Taper ratio	$TR = c_{tip} / c_{root}$
angle	Sweep back angle	$angle = \alpha$
DR	Relative distance of wing's root from glider's nose	$DR = d / c_t$
Body parameters		
n_1, n_2, n_3,	Relative spanwise coordinate of the control points	$n_i = z_i / b_t \quad i = 1,2,3$
CR	Relative body chord at the centerline	$CR = c_t / b_t$

Parameters of section

Typical symmetrical airfoil NACA 0012 is used as a baseline airfoil. As shown in Fig. 3, any section of the airfoil is designed with changing thickness of NACA 0012 (= 12.0% *c*, *c* is the chord length of local section). Thickness is defined at the centerline ($t_1 \cdot c$), the merging point ($t_2 \cdot c$), and the section between the centerline and the merging point ($t_{body} \cdot$c) as shown in Fig. 3. To maintain spanwise monotonic distribution of the relative thickness, t_{body} is decided by following equation.

$$t_{body} = \left(1 - \frac{z}{n_3}\right) \cdot t_1 + \frac{z}{n_3} \cdot t_2 \qquad \left(0 \le z \le n_3\right) \tag{1}$$

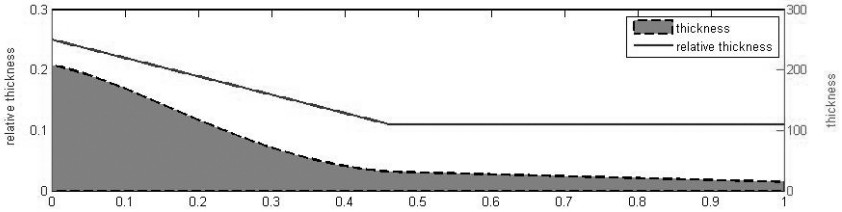

Fig. 3 Spanwise distribution of the relative thickness.

NUMERICAL METHOD

The hydrodynamic numerical simulations of BWB underwater glider presented in this paper were carried out using the commercial code Fluent, based on finite volume method. The fluid material selected in this paper was the water-liquid which was considered incompressible with a density of 998.2 kg/m^3 and a dynamic viscosity of 1.003×10^{-3} $Pa\cdot s$. The turbulence model selected in this paper is the k-ω SST model.

Governing equations

The governing equations for the cases considered in this report are the Navier-Stokes equations for incompressible viscous flow, and a statistically steady solution is found. The Navier-Stokes equations including the continuity equation and momentum equation are given below:

$$\frac{\partial \rho}{\partial t}+\nabla \rho \vec{v}=0 \tag{2}$$

$$\frac{\partial}{\partial t}(\rho \vec{v})+\nabla(\rho \vec{v}\vec{v})=-\nabla p+\nabla \bar{\bar{\tau}}+\vec{F} \tag{3}$$

where ρ is the density of fluid ,the vector v is the relative velocity, p is the pressure, the vector $\bar{\bar{\tau}}$ refers to the stress tensor and the vector F is external body forces.

Computational domains and grid generation

The shape of the computational domain is a cuboid as shown in Fig. 4. The inlet velocity at the front of the fluid domain was set to be equivalent to the glider velocity, 2 *m/s*. The pressure outlet at the end of the fluid domain was set to be 0 *Pa*. To reduce the computational cost, this simulation utilizes a symmetry plane in a *xy*-plane through the center of the glider. The wall condition was allocated to other surfaces of the fluid domain. Using the chord length at the center (c_t) as the reference length, the domain is [-10c_t, 15c_t] m × [-10c_t, 10c_t] m × [0, 10c_t] m with 2.3 million hexahedral cells. The glider is placed at the origin of the coordinates.

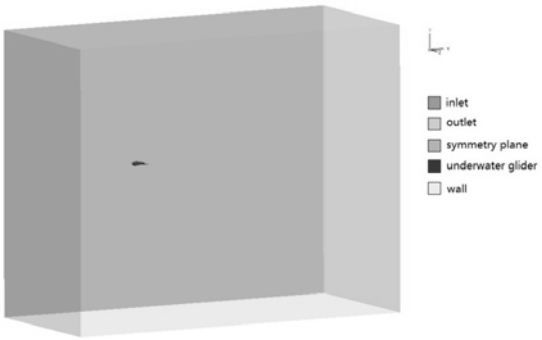

Fig. 4 The computational domain.

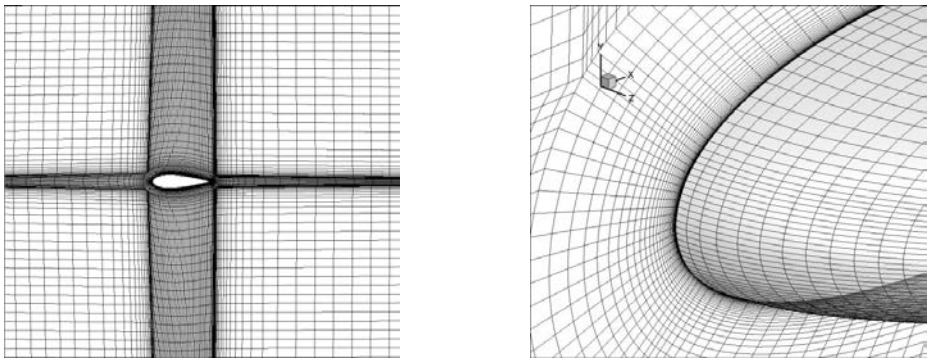

(a) (b)

Fig. 5(a) grid structure in the symmetry plane (b) Detail of the boundary layers near the glider body.

Structured grids with hexahedral cells are used in all the calculations presented here. Fig. 5(a) shows the grid structure in the symmetry plane through the middle of the glider. As shown in Fig. 5(b), the o-blocks around the glider are used to make the grids closest to the profiles of the glider become dense. The first element height of cells adjacent to the body was set to less than 5 *y*+ (White, 2008) units for compatibility with the k-ω SST turbulence model.

Numerical method validation

In order to validate the accuracy of the hydrodynamic numerical simulations used in this paper, we performed simulation of the airfoil NACA0012 which was used in this paper. Simulations are conducted for $Re = 10^6$ in water. Coefficients for lift, drag, and lift to drag ratio are given in Fig. 6 and compared with the experimental data (Abbott, 1959) for $Re = 10^6$.

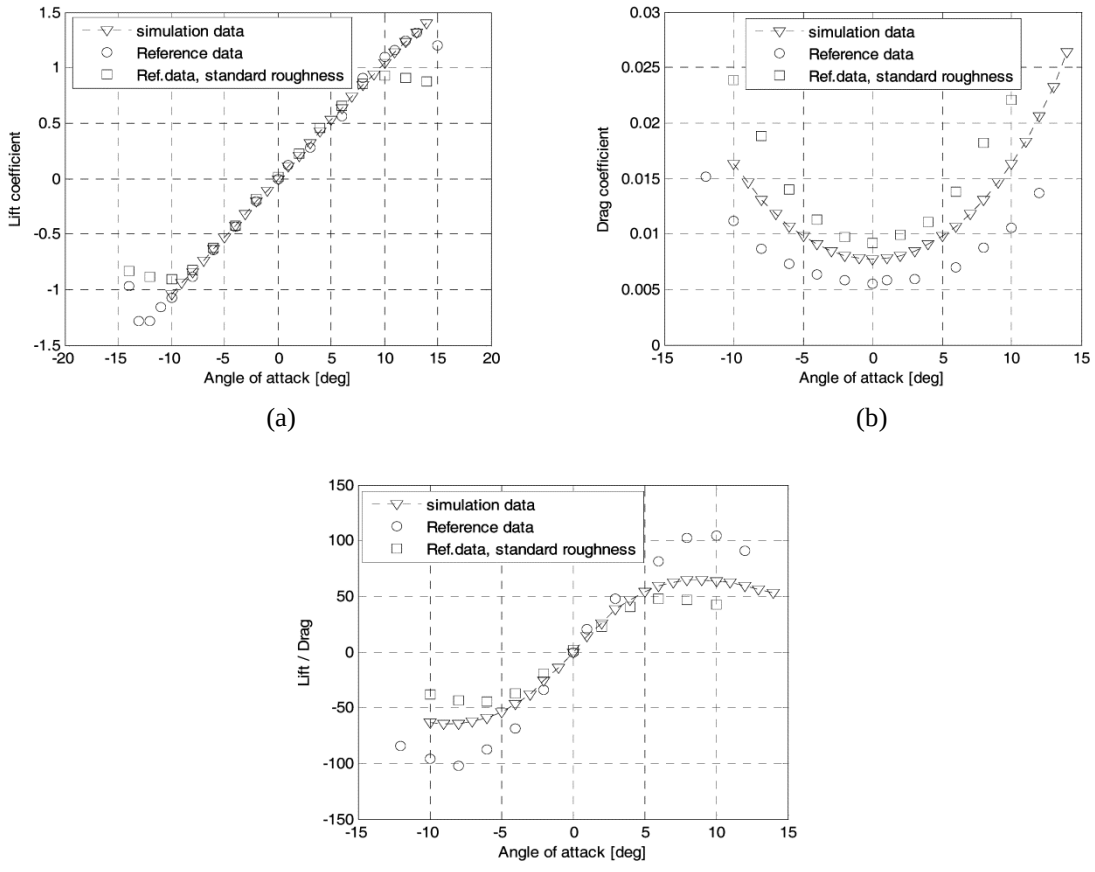

(a) (b)

(c)

Fig. 6 NACA-0012 airfoil: (a) lift coefficient, (b) drag coefficients, (c) lift to drag ratio.

As shown in Fig. 6, the lift characteristic is shown to be in good agreement with the experimental data, but the drag characteristic not. That's because these experimental data are obtained using an untripped airfoil (NASA Langley Research Center, 2014), i.e. the boundary layer is not fully turbulent over the wing, but contains a laminar turbulent transition, which reduces the drag, especially for small and moderate attack angles. It is virtually impossible to simulate such a transition using available models in Fluent, so it is inherently assumed in the simulations that the boundary layer is fully turbulent everywhere. For application to underwater systems, this is probably a more realistic scenario. However, data for a "standard roughness" wing at Re =10^6 are also given in the experimental data (Abbott, 1959). This can be considered a "worst case" roughness for an airplane wing, so it seems reasonable that the calculated drag coefficients lie between the two extremes of untripped and standard roughness data.

EFFICIENT GLOBAL OPTIMIZATION (EGO)

Kriging model

The Kriging model expresses the unknown function $\hat{y}(\mathbf{x})$ as

$$\hat{y}(\mathbf{x}) = \beta + Z(\mathbf{x}) \tag{4}$$

where x is an n-dimensional vector (n design variables), β represents a linear regression part. $Z(\mathbf{x})$ represents a local deviation from the global model, and $Z(\mathbf{x})$ is a model of a Gaussian and stationary random process with zero mean and covariance:

$$E[Z(\mathbf{x})] = 0 \tag{5}$$

$$E[Z(\mathbf{x})Z(\mathbf{x}_i)] = \sigma^2 R(\mathbf{x}, \mathbf{x}_i) \tag{6}$$

where σ^2 is the variance of stationary random process. $R(\mathbf{x}, \mathbf{x}_i)$ is the spatial correlation function which represents the correlation between $Z(\mathbf{x})$ and $Z(\mathbf{x}_i)$, and it is related to the distance between the two corresponding points x and xi. The Spatial Correlation Function (SCF) is defined as:

$$R(\mathbf{x}, \mathbf{x}_i) = \exp[-d(\mathbf{x}, \mathbf{x}_i)] \tag{7}$$

$$d(\mathbf{x}, \mathbf{x}_i) = \sum_{k=1}^{n} \theta_k (x_{ki} - x_k)^2 \tag{8}$$

where, $d(\mathbf{x}, \mathbf{x}_i)$ is a special weighted distance, $\theta_k (\theta_k > 0)$ is the k*th* element of correlation vector parameter $\boldsymbol{\theta}$. According to the spatial correlation function, the correlation matrix can be defined as:

$$\mathbf{R} = \begin{bmatrix} R(\mathbf{x}_1, \mathbf{x}_1) & R(\mathbf{x}_1, \mathbf{x}_2) & \cdots & R(\mathbf{x}_1, \mathbf{x}_N) \\ R(\mathbf{x}_2, \mathbf{x}_1) & R(\mathbf{x}_2, \mathbf{x}_2) & \cdots & R(\mathbf{x}_2, \mathbf{x}_N) \\ \vdots & \vdots & \ddots & \vdots \\ R(\mathbf{x}_N, \mathbf{x}_1) & R(\mathbf{x}_N, \mathbf{x}_2) & \cdots & R(\mathbf{x}_N, \mathbf{x}_N) \end{bmatrix} \tag{9}$$

Each element of this matrix $\mathbf{R}$ is a spatial correlation function of two known points, and this matrix $\mathbf{R}$ shows each possible

combination of all known points. The correlation between an unknown point *x* and the N known sample points is represented by a vector **r(x)** :

$$\mathbf{r(x)} = \left\{ R(\mathbf{x}, \mathbf{x}_1) \quad R(\mathbf{x}, \mathbf{x}_2) \quad \cdots \quad R(\mathbf{x}, \mathbf{x}_N) \right\}^T \tag{10}$$

In this paper, we just give the final equations for Kriging formulation, while the more details regarding their development can be found in Martin (2005). The Kriging predictor $\hat{y}(\mathbf{x})$ is

$$\hat{y}(\mathbf{x}) = \hat{\boldsymbol{\beta}} + \mathbf{r}^T(\mathbf{x})\mathbf{R}^{-1}(\mathbf{Y} - \mathbf{E}\hat{\boldsymbol{\beta}}) \tag{11}$$

where $\boldsymbol{Y}$ is N-dimensional vector, and $\hat{\boldsymbol{\beta}}$ is the least-squares estimated of β :

$$\mathbf{Y} = \left\{ y(\mathbf{x}_1) \quad y(\mathbf{x}_2) \quad \ldots \quad y(\mathbf{x}_N) \right\}^T \tag{12}$$

$$\hat{\boldsymbol{\beta}} = (\mathbf{E}^T\mathbf{R}^{-1}\mathbf{E})^{-1}\mathbf{E}^T\mathbf{R}^{-1}\mathbf{Y} \tag{13}$$

The Kriging predictor $\hat{y}(\mathbf{x})$ has uncertainty, and this uncertainty is expressed as

$$\mathrm{MSE}\left[\hat{y}(\mathbf{x})\right] = \sigma^2 \left\{ 1 - \mathbf{r}^T(\mathbf{x})\mathbf{R}^{-1}\mathbf{r}(\mathbf{x}) + \left[1 - \mathbf{E}^T\mathbf{R}^{-1}\mathbf{r}(\mathbf{x}) \right]^2 \left(\mathbf{E}^T\mathbf{R}^{-1}\mathbf{E} \right)^{-1} \right\} \tag{14}$$

where s^2 is the mean squared error of $\hat{y}(\mathbf{x})$, and it indicates the uncertainty at the point *x*. When point x into sample point, the value of s^2 converges to zero. This means that the uncertainty of the estimation point largely depends on the distance from sample points, in other words, the farther point *x* to the sample point, the more uncertain is the prediction $\hat{y}(\mathbf{x})$.

Expected improvement (EI)

EGO method uses expected improvement EI as a highly attractive figure of merit to balance local and global search. The EI is computed as follows. Let $f_{\max} = \max(y_1, \cdots, y_n)$ be the current best function value. The improvement at the point *x* is expressed as $I(\mathbf{x}) = \max(Y - f_{\max}, 0)$ where *Y* is a random variable because the Kriging predictor $\hat{y}$ has uncertainty.

The expected improvement is:

$$\mathrm{E}\left[I(\mathbf{x}) \right] = \mathrm{E}\left[\max\left(Y - f_{\max}, 0 \right) \right] \tag{15}$$

To compute this expectation, *Y* is defined as a normal distribution, and *Y* is $N(\hat{y}, s^2)$. $\hat{y}$ is the Kriging predictor and s is its standard error at x. The expected improvement can be expressed as

$$\mathrm{E}\left[I(\mathbf{x}) \right] = \left(\hat{y} - f_{\max} \right) \Phi\left(\frac{\hat{y} - f_{\max}}{s} \right) + s\phi\left(\frac{\hat{y} - f_{\max}}{s} \right) \tag{16}$$

where Φ is the standard distribution, and ϕ is normal density. According to Eq. (16), the maximum EI point means the optimal point or the maximum uncertainty point in the Kriging model. The maximum EI point as additional sample point is used to update the Kriging model, and this process is iterated until the maximum EI close to zero.

Genetic algorithm (GA)

Optimization of hydrodynamic shape is a complex problem where nonlinearity, multimodality, and discontinuities may exist. The value of objective function can be obtained by CFD, but the derivative (gradient) information can't be obtained easily. GA (Golberg, 1989) which is based on natural selection theory only use the value of objective function without the gradient information. This feature makes GA become an efficient search mechanism for hydrodynamic shape design. Fig. 7 shows the general procedure of GA:

1. Creating initial population,
2. Calculating fitness (objective) functions,
3. Checking whether the fitness satisfies the termination condition. If not satisfied, turn to next step,
4. Selection of parents according to the rank (fitness),
5. Crossover and mutation, creating new population and return to step 2.

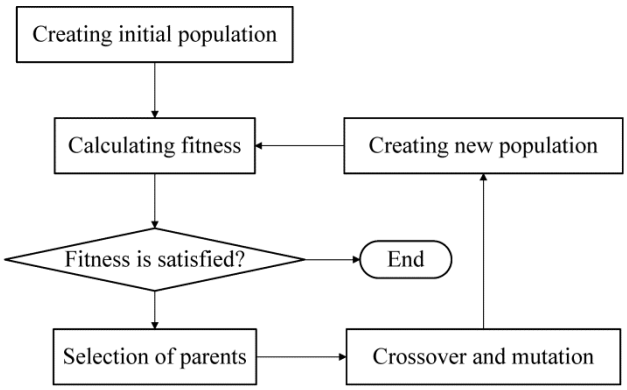

Fig. 7 Illustrates the general procedure of GA.

Optimization procedure

The Efficient Global Optimization (EGO) is a Kriging-based genetic algorithm. Fig. 8 shows the optimization procedure. First, N design samples are selected using Latin Hypercube Sampling (LHS). The hydrodynamic performance of N samples is evaluated using numerical simulations. Second, the initial Kriging model is constructed based on N sample data. Then, GA searches the Expected Improvement (EI) maximum point based on the predicted value by the initial Kriging model. Finally, the performance of the EI maximum point is evaluated by numerical simulations, and the Kriging model is updated with N+1 sample data. This process is iterated until the objective functions are not improved any more. Each step of the optimization procedure is described in detail in the following sections.

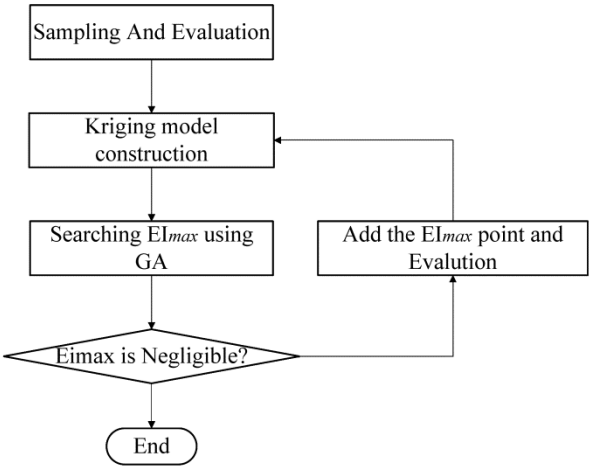

Fig. 8 Procedure for the efficient exploration of the global design model.

RESULTS AND DISCUSSION

According to the parametric design of BWB underwater glider, Table 2 shows the parameter ranges of design space which was determined by avoiding abnormal shape.

Table 2 Parameter ranges of design space.

Parameter	Lower bound	Upper bound
n_1	0.12	0.18
n_2	0.25	0.38
n_3	0.3	0.6
AR	1	1.5
CR	0.3	0.7
DR	0.3	0.6
TR	0.2	0.4
angle	30°	40°
t_1	0.09	0.15
t_2	0.20	0.30

The number and distribution of sample points are important factors which affect the accuracy of the Kriging model. The number of sample points should be so sufficient that these points can be spread over the design space uniformly. In this paper, the initial 45 samples were selected by LHS and the performance of 45 samples was evaluated by the commercial code Fluent. The initial Kriging model was then constructed based on this sample data. As already discussed, the objective function *L*/*D* was transformed to the EI to avoid missing the global maximum point. The objective functions are expressed as follows:

$$\mathrm{E}\left[I(\mathbf{x})\right] = (\hat{y} - L/D)\Phi\left(\frac{\hat{y} - L/D}{s}\right) + s\phi\left(\frac{\hat{y} - L/D}{s}\right) \tag{17}$$

The maximum EI point as an additional sample was found by GAs. Then, the *L*/*D* of additional sample was evaluated by Fluent and the new Kriging model was built with 46 sample data. This process is iterated until the maximum *L*/*D* was not improved any more. After 12 additional samples, there was no *L*/*D* improvement.

Table 3 Optimization results: comparison of hydrodynamic performance.

	Optimal design	Initial design	Slocum	Spray	Seaglider
Maximum L/D	18.73	17.49	6.85	6.23	4.44
Angle of attack (*deg.*)	5.78	5.53	9.38	12.27	13.36

The optimum value, the initial value and the Simulation values (Jenkins et al., 2003) of three conventional under water gliders are shown in Table 3. The maximum *L*/*D* is 18.73, and it is 7% higher than the initial design. The maximum *L*/*D* of the BWB underwater glider is obviously higher than that of three conventional underwater gliders. This result shows that geometry definition, CFD and EGO process successfully optimized the initial design. Fig. 9 shows the pressure distribution around the optimum and initial design. The optimized the initial design has a similar pressure distribution that the low pressure area is appeared around the leading edge of the upper surface at the merging point and the high pressure area is appeared at lower surface of the wing.

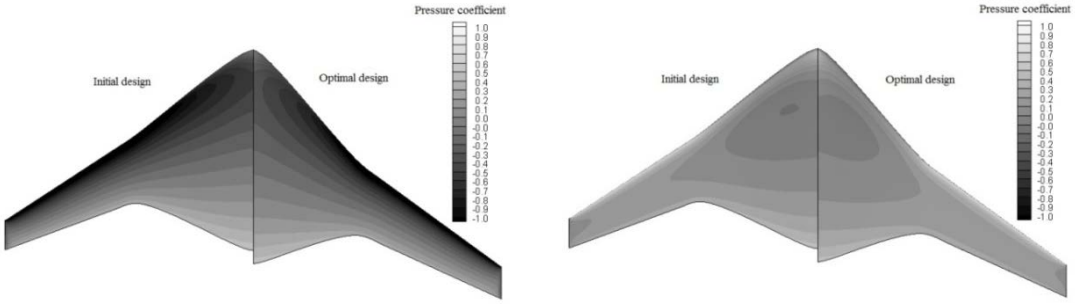

(a) (b)

Fig. 9 Pressure distributions around the optimum and initial design: (a) upper surface, (b) lower surface.

Fig. 10 shows the relative sensitivities of the design variables. According to the sensitivities, *L*/*D* is sensitive to the change of t_2, t_1, n_1, n_2 and angle, and is insensitive to the change of other design variables. This mains that the relative thickness of section and the shape of Bezier curve are important factors affecting the hydrodynamic performance.

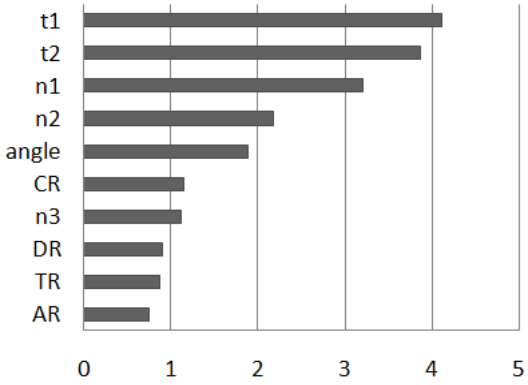

Fig. 10 Sensitivity of *L*/*D* to changes in the design variables.

Fig. 11 illustrates two kinds of the two-way interactions which contain 45 kinds of combinations. Fig. 11(a) is about t_2 vs. n_3 and these two design variables determine the relative thickness and relative location of the merging section. According to Fig. 11(a), when the merging point is placed at the 40%-50% semispan and the relative thickness varies between 1 and 1.1, the design has better hydrodynamic performance. Fig. 11(b) is about t_1 vs. n_1 and these two design variables determine the relative thickness of the centerline section and sharpness of the nose. According to Fig. 11(b), it is found that the design which has sharper nose (lower n_1) and thinner airfoil of the centerline (lower t_1) achieves higher hydrodynamic performance.

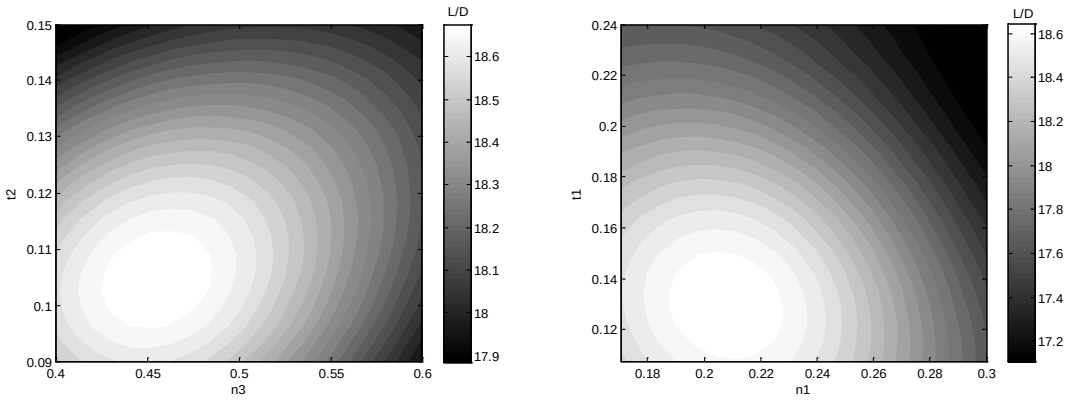

(a) (b)

Fig. 11 Design variables two-way interactions: a) $t_2$vs.n_3, b) $t_1$vs.n_1.

CONCLUSIONS

In this paper, the shape of a new under water glider was designed with the Blended-Wing-Body (BWB) configuration, and the parametric geometric model of this underwater glider has been built with 10 design variables. The hydrodynamic performance of the BWB underwater glider was evaluated using a Navier-Stokes code. The Efficient Global Optimization (EGO) was used to solve the hydrodynamic design optimization which has expensive black-box functions. By summarizing the results of this study, we conclude as follows.

1) The hydrodynamic performance of the BWB underwater glider is obviously better than that of conventional under water glider such as Slocum Battery/Thermal glider, the Stingray (or Manta) glider and the Sea-glider.
2) The lift to drag ratio of initial design has been enhanced by 7%in the EGO process.
3) The sensitivity of the lift to drag ratio to each of the design variables was analysed, and according to the result, it was found that the relative thickness of airfoil and sharpness of the nose are important factors affecting the hydrodynamic performance.

In this paper, the BWB underwater glider has been designed without considering the control surfaces. Actually, the vertical control surfaces (winglets) effectively reduce the induced drag. The design and optimization of the winglets will be taken into account in the future research.

ACKNOWLEDGEMENTS

This research was supported by the National Science Foundation of China (Grant No. 51375389) and the Doctorate Foundation of Northwestern Polytechnical University.

REFERENCES

Abbott, I. H., 1959. *Theory of wing sections, including a summary of airfoil data*. New York: Courier Dover Publications.

Bachmayer, R., Leonard, N.E., Graver, J., Fiorelli, E., Bhatta, P. and Paley, D., 2004. Underwater gliders: Recent developments and future applications. *Proceedings of IEEE International Symposium Underwater Technology*, Taipei, April 2004, pp.195-200.

Center, N.L.R., 2014. *Turbulence modeling resource.*[Online]. http://turbmodels.larc.nasa.gov/. NASA Langley Research Center.

Crane, D., 2012. *Dictionary of aeronautical terms*. New York:Aviation Supplies & Academics, Incorporated.

Eriksen, C.C., Osse, T.J., Light, R.D., Wen, T., Lehman, T.W., Sabin, P.L., Ballard, J.W. and Chiodi, A.M., 2001. Seaglider: A long-range autonomous underwater vehicle for oceanographic research. *IEEE Journal of Oceanic Engineering*, 26, pp.424-436.

Farin, G. and Kim, H.M.S., 2002. Handbook of computer aided geometric design. *North-Holland, Amsterdam*, 18, pp.771-795.

Golberg, D.E., 1989. *Genetic algorithms in search, optimization, and machine learning*. California:Addion wesley.

Graver, J.G., 2005. *Underwater gliders: dynamics, control and design.* Ph. D. Thesis. Princeton University.

Hildbrand, J.A., Spain, D., Gerald, L. and Rosh, M.A., 2011. *Glider-based passive acoustic monitoring techniques in the southern california region*. New Jersey: DTIC Document.

Huggins, A. and Packwood, A.R., 1995. Wind tunnel experiments on a fully appended laminar flow submersible for oceanographic survey. *Ocean Engineering*, 22(2), pp.207-221.

Jenkins, S.A., Humphreys, D.E., Sherman, J., Osse, J., Jones, C., Leonard, N., Graver, J., Bachmayer, R., Clem, T. and Carroll, P., 2003. *Underwater glider system study*. *Arlington: Scripps Institution of Oceanography*.

Jeong, S., Murayama, M. and Yamamoto, K., 2005. Efficient optimization design method using kriging model. *Journal of Aircraft*, 42(2), pp.413-420.

Li, P., Zhang, B., Chen, Y., Yuan, C. and Lin, Y., 2012. Aerodynamic design methodology for blended wing body transport. *Chinese Journal of Aeronautics*, 25(4), pp.508-516.

Liebeck, R.H., 2004. Design of the blended wing body subsonic transport. *Journal of Aircraft*, 41(1), pp.10-25.

Ma, Z., Zhang, H., Zhang, N. and Ma, D.M., 2006. Study on energy and hydrodynamic performance of the underwater glider. *Journal of Ship Mechanics*, 10, pp.53-60.

Martin, J.D., 2005. Use of kriging models to approximate deterministic computer models. *AIAA Journal*, 43(4), pp.853-863.

Mohr, B., Paulus, D., Baier, H. and Hornung, M., 2012. Design of a 450-passenger blended wing body aircraft for active control investigations. *Proceedings of the Institution of Mechanical Engineers, Part G: Journal of aerospace engineering*, 226, pp.1513-1522.

ONR, 2006. *Liberdade XRAY advanced underwater glider* [Online]. https://www.onr.navy.mil/media/extra/fact_sheets/advanced_underwater_glider.pdf. U.S. Office of Naval Research.

Peigin, S. and Epstein, B., 2006. Computational fluid dynamics driven optimization of blended wing body aircraft. *AIAA Journal*, 44(11), pp.2736-2745.

Potsdam, M.A., Page, M.A. and Liebeck, R.H., 1997. Blended wing body analysis and design. *15th AIAA applied aerodynamics conference*, California, June 1997, pp.799-805.

Prautzsch, H., Boehm, W. and Paluszny, M., 2002. *Bézier and B-spline techniques*. New York: Springer.

Sherman, J., Davis, R.E., Owens, W.B. and Valdes, J., 2001. The autonomous underwater glider "spray". *IEEE Journal of Oceanic Engineering*, 26, pp.437-446.

Stevenson, P., Furlong, M. and Dormer, D., 2009. AUV design: shape, drag and practical issues. *Sea Technology*, 50, pp. 41-44.

Stommel, H.M., 1989. The slocum mission. *Oceanus*, 32, pp.93-96.

Webb, D.C., Simonetti, P.J. and Jones, C.P., 2001. Slocum: an underwater glider propelled by environmental energy. *IEEE Journal of Oceanic Engineering*, 26, pp.447-452.

Whie, F.M., 2008. *Fluid mechanics*. 4th. New York: McGraw-Hill.